Microchimica Acta (2019) 186: 757
https://doi.org/10.1007/s00604-019-3883-x

ORIGINAL PAPER

A microfluidic immunosensor for visual detection of foodborne bacteria using immunomagnetic separation, enzymatic catalysis and distance indication

Gaozhe Cai[1] · Lingyan Zheng[2] · Ming Liao[3] · Yanbin Li[4] · Maohua Wang[2] · Ning Liu[1] · Jianhan Lin[1,2]

Received: 28 May 2019 / Accepted: 29 September 2019 / Published online: 9 November 2019

Abstract

A disposable visual microfluidic immunosensor is described for the determination of foodborne pathogens using immunomagnetic separation, enzymatic catalysis and distance indication. Specifically, a sensor was designed to detect *Salmonella* typhimurium as a model pathogen. Magnetic nanoparticles (MNPs) were modified with the anti-*Salmonella* monoclonal antibodies and then used to enrich *S. typhimurium* from the sample. This is followed by conjugation to polystyrene microspheres modified with anti-*Salmonella* polyclonal antibodies and catalase to form the MNP-bacteria-polystyrene-catalase sandwich. The catalase on the complexes catalyzes the decomposition of hydrogen peroxide to produce oxygen after passing a micromixer. The generated oxygen gas increases the pressure in the chip and pushes the indicating red dye solution to travel along the channel towards the unsealed outlet. The travel distance of the red dye can be visually read and related to the amount of *S.* typhimurium using the calibration scale. The sensor can detect as low as 150 CFU·mL^{-1} within 2 h.

Keywords Microfluidics · Distance readout · Pathogens detection · Enzymatic catalysis · Magnetic nanoparticles · Polystyrene microspheres · Catalase · Hydrogen peroxide · Chicken samples

Introduction

Food safety has received a growing concern globally, since the outbreaks of foodborne illnesses caused by the consumption of foods contaminated with pathogenic bacteria has drastically increased in the past decade [1]. According to the report of the World Health Organization (WHO) in 2017, diarrheal, one of the most common foodborne illnesses, had caused 550 million illnesses and 230,000 deaths every year [2]. Foodborne illnesses are often caused lots of pathogenic bacteria, such as *Campylobacter*, *Salmonella*, *Escherichia coli* O157:H7 and *Listeria monocytogenes* [3]. Therefore, rapid and sensitive detection of foodborne pathogenic bacteria has become more and more important to ensure food safety.

The current methods for detection of foodborne pathogenic bacteria mainly include the gold standard culture plating (Culture) [4], polymerase chain reaction (PCR) [5–7], and enzyme linked immunosorbent assay (ELISA) [8, 9]. Culture has been used for decades due to its high sensitivity and accuracy. However, it generally requires 2–3 d to obtain the results due to such multiple steps such as pre-enrichment, selective enrichment, selective plating, biochemical screening and serological confirmation. PCR reduces the detection time from days to hours (3–6 h) with good sensitivity and specificity, but with complex DNA extraction procedure and expensive equipment [10]. ELISA is fast and high-throughput, however conventional ELISA in the plate often lacks sufficient sensitivity and has a relative high false positive ratio. Hence,

Electronic supplementary material The online version of this article (https://doi.org/10.1007/s00604-019-3883-x) contains supplementary material, which is available to authorized users.

✉ Jianhan Lin
jianhan@cau.edu.cn

[1] Key Laboratory of Agricultural Information Acquisition Technology, Ministry of Agriculture and Rural Affairs, China Agricultural University, Beijing 100083, China

[2] Key Laboratory of Modern Precision Agriculture System Integration Research, Ministry of Education, China Agricultural University, Beijing 100083, China

[3] College of Veterinary Medicine, South China Agricultural University, Guangzhou 510642, China

[4] Department of Biological and Agricultural Engineering, University of Arkansas, Fayetteville, AR 72701, USA

visual bacterial detection methods with shorter detection time, higher sensitivity and simpler operation are urgently required.

In the past decade, various biosensors based on optical methods [11–13], electrochemical methods [14], magnetic methods [15, 16], and piezoelectric methods [17, 18], etc., have drawn increasing attentions due to their rapid response, high sensitivity, simple operation and low cost. However, most of these biosensors still require expensive or cumbersome equipment, which was not suitable for in-field detection. Distance-based biosensors have been demonstrated as a desirable detection method for rapid and in-field applications and have shown some advantages over traditional methods, such as small size, low cost, simple operation and rapid detection. Relying on the position change of the visible color indicator that is linear with the concentration of the targets, the distance-based biosensors can realize quantitative results visually. The microfluidic paper-based analytical devices (μPADs) were often used as one of the distance-based biosensors due to their advantages of low cost, easy fabrication and free pump requirement [19]. These biosensors are ideal for rapid detection of foodborne pathogens in remote areas and developing countries, where professional technicians are often lack, and are suitable for qualitative tests [20]. As one type of the distance-based microfluidic biosensors, the volumetric bar-chart chips based on slip chip technology [21] have been often reported for equipment-free, visible and quantitative detection of some biomarkers, such as DNA, cancer cells, and myoglobin. However, these chips generally required a complex process for the glass, including washing with piranha solution, silanizing and oil treatment, and they were often expensive due to the use of the photolithography and wet etching for fabrication. Some low-cost and simple distance-based microfluidic chips were also reported. Xie et al. developed a Shake&Read microfluidic chip for the detection of the prostate specific antigen in serum [22]. After the simply shaking microfluidic chip by hand, H_2O_2 and the sample were incubated in the reaction chamber and the biomarker of the prostatic cancer was directly detected visually. Liu et al. reported an ELISA microfluidic chip for visible and quantitative detection of inflammatory biomarker C-reaction protein [23], which integrated the entire ELISA process with the distance readout. These distance-based microfluidic biosensors had shown their merits for in-field applications, however their reproducibility was still unsatisfied due to the complex and manual operations.

In this study, we proposed a portable and low-cost microfluidic immunosensor based on immunomagnetic separation, enzymatic catalysis and distance indication for quantitative detection of foodborne bacteria. As shown in Fig. 1, the anti-*Salmonella* monoclonal antibodies (mAbs) conjugated magnetic nanoparticles (MNPs) were first used to separate *S.* typhimurium from the sample and form the MNP-*Salmonella* complexes. The polystyrene microspheres (PSs) conjugated with the anti-*Salmonella* polyclonal antibodies (pAbs) and the catalases were then reacted with the MNP-*Salmonella* complexes to form the MNP-*Salmonella*-PS-catalase complexes. After magnetic separation to remove the redundant PSs, these complexes were re-suspended with PBS and pipetted into the sample chamber of the microfluidic immunosensor. Then, the press chamber was precisely squeezed using the 3D-finger controlled by the stepper motor for driving both these complexes and the pre-filled hydrogen peroxide to pass through the split-and-recombine micromixer to the reaction chamber. Due to the catalysis of H_2O_2 to produce O_2 by the catalases on the complexes, the increasing pressure in the reaction chamber pushed the pre-filled red dye solution to travel along the serpentine indication channel with scale towards the open outlet. Finally, the travel distance of the red dye was read visually and used to determine the concentration of the *Salmonella* cells.

Materials and methods

Materials

The monoclonal and polyclonal antibodies against *Salmonella* were purchased from Abcam (ab69255, Cambridge, MA, US, https://www.abcam.com) and Meridian (C86309M, Memphis, TN, USA, https://meridianlifescience.com), respectively. The carboxyl modified magnetic nanoparticles (MNPs) with the average diameter of 150 nm and the Fe concentration of 1 $mg{\cdot}mL^{-1}$ were purchased from Ocean Nanotech Co., Ltd. (San Diego, CA, US, https://www.oceannanotech.com). The carboxyl modified polystyrene microspheres (PSs) with the diameter of 1 μm and the concentration of 50 $mg{\cdot}mL^{-1}$ were obtained from Bangs laboratories (Fishers, Indiana, US, https://www.bangslabs.com). 1-ethyl-3-(3-dimethylaminopropyl)-carbodiimide hydrochloride (EDC) and the mineral oil were purchased from Sigma Aldrich (St. Louis, MO, US, https://www.sigmaaldrich.com). Phosphate-buffered saline (PBS) (P5493, 10 times concentrated) from Sigma Aldrich were diluted 10 times by the deionized water to prepare the PBS (pH 7.4, 0.01 M). Luria-Bertani (LB) medium was purchased from Aoboxing Biotech Co., Ltd. (Beijing, China, http://www.abxing.com.cn). Hydrogen peroxide (H_2O_2) was obtained from Aladdin (Shanghai, China, https://www.aladdin-e.com). Bovine serum albumin (BSA) was purchased from EM Science (Gibbstown, NJ, US, http://www.emscience.com). The red and blue dye for indicating was purchased from Shanghai Hero Co., Ltd. (Shanghai, China, http://www.hero.com.cn) and diluted 5 times by DI water prior to use. PBST (PBS containing 0.05% Tween 20) was prepared for

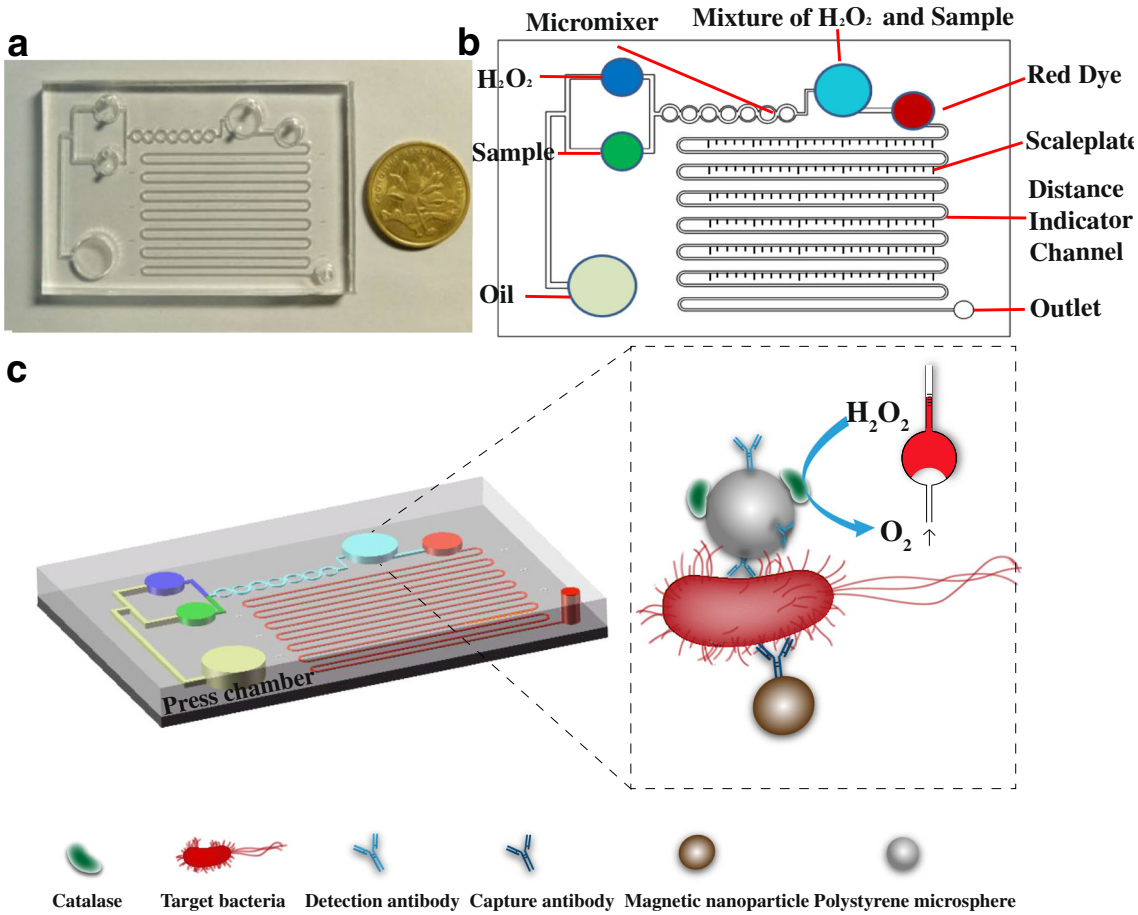

Fig. 1 **a** Photograph of the microfluidic immunosensor **b** Schematic diagram of the top view of the microfluidic immunosensor **c** The principle of the microfluidic immunosensor for rapid detection of foodborne pathogenic bacteria

washing. The deionized water produced by Advantage A10 from Millipore (Burlington, MA, US, http://www.merckmillipore.com) was used for preparing all the solutions.

The silicone elastomer kit for fabricating the microfluidic chip was purchased from Dow Corning (Sylgard 184, Auburn, MI, US, https://consumer.dow.com/en-us.html). The 3D printer (Object 24) and the printing material (VeroWhite plus RGD835) were purchased from Stratasys (Eden Prairie, MN, US, https://www.stratasys.com). The stepper motor kit from Ketedi 3D studios (A4988, Guangdong, China, https://m.tb.cn/h.e9tyxn3) was used with the driver to construct the 3D-printed finger for squeezing the press chamber. The pressure meter (HT-1890) was purchased from Dongguan Xintai Instrument Co., Ltd. (Guangdong, China, https://xintest.en.alibaba.com/).

Design and fabrication of the microfluidic immunosensor

The microfluidic immunosensor included a PDMS microfluidic chip for detection of the bacteria, a 3D-printed finger with a stepper motor for precisely squeezing the press chamber instead of manual operation, and a poly(methyl methacrylate) (PMMA) frame for fixing the microfluidic chip. The picture of this immunosensor can be found in Fig. S1 in the supplemental material. The microfluidic chip with 4 mm thick PDMS was the most important part of the immunosensor. It consisted of five parts: (1) a press chamber with the diameter of 8.0 mm and the height of 2.5 mm, which was prefilled with oil, for driving the sample and hydrogen peroxide; (2) a passive split-and-recombine micromixer with multiple asymmetric rings for rapid and efficient mixing of the sample and H_2O_2; (3) three storage chambers with the diameter of 3.5 mm and the height of 1.1 mm for storing 20 μL of the sample, H_2O_2 and red dye, respectively; (4) a reaction chamber with the diameter of 7.0 mm and the height of 1.1 mm for catalyzing H_2O_2 into O_2; (5) a distance indication channel with the width of 300 μm and the height of 150 μm, which was connected with a dye chamber with the diameter of 5.0 mm and the height of 1.1 mm, for visually indicating the results. A hole was set on the top of each chamber for pipetting the relevant solution. The red dye purchased from Shanghai Hero (Shanghai, China) was pre-filled in the dye chamber before each experiment to indicate the travel distance due to

the pressure change caused by the oxygen from the enzymatic reaction. The passive micromixer was designed according to the previous study reported by Ansari [24] and scaled up in equal proportion. The detailed parameters of the micromixer ($w = 0.6$ mm, $L_0 = 1$ mm, $Pi = 2.4$ mm, and $w_1/w_2 = 2$) can be found in Fig. S1 in the supplemental material. It is worth mentioning that the size of the outlet of the micromixer (i.e. the inlet of the reaction chamber) was 0.3 × 0.2 mm (width × height), which was 3 times smaller than that of the outlet of the reaction chamber (0.6 × 0.3 mm), to avoid the backflow in the reaction chamber.

The mold of this microfluidic chip was designed using Solidworks software (Concord, MA, US) and fabricated by the Objet24 3D printer. Then, the PDMS prepolymer and the curing agent were mixed at a mass ratio of 8:1 for 10 min and casted onto the mold after degassing in vacuum for 20 min, followed by curing at 60 °C overnight. Finally, the PDMS channel was removed from the mold and bonded on a clean glass using oxygen plasma treatment (Harrick Plasma, Ithaca, NY, US, https://harrickplasma.com).

Culture and enumeration of the bacterial cells

Salmonella Typhimurium (target bacteria), *Listeria monocytogenes* (non-target bacteria), *Salmonella* derby (non-target bacteria), *Salmonella* enteritidis (non-target bacteria) and *Escherichia coli* O157:H7 (non-target bacteria) were cultured at 37 °C for 12–16 h in the LB medium with a shaking speed of 180 rpm before each assay. Different concentrations of bacteria suspensions were prepared with PBS. For bacteria enumeration, the bacterial samples were serially diluted with PBS and 100 μL of diluents were surface plated on the LB agar plates. After incubating at 37 °C for 22–24 h, the bacteria were counted to calculate the concentration.

Preparation of the spiked chicken samples

Packages of fresh boneless chicken breast were purchased from a local supermarket in Beijing. According to the food safety national standards, 25 g of the chicken breast was first added into 225 mL of PBS and homogenized for 4 min using the stomacher (BagMixer CC, InterScience, Paris, France, https://www.interscience.com). After standing for 5 min, the supernatant was collected and *S.* Typhimurium was then added into it to prepare the spiked chicken samples with the bacteria concentrations from 1.2×10^2–1.2×10^6 CFU·mL^{-1}.

Preparation of the catalase and pAbs modified polystyrene microspheres (PSs)

According to the report by Chen et al. [25], 20 μL of the PSs (50 mg·mL^{-1}) were first centrifuged at 7000 rpm for 10 min to remove the background and re-suspended with 25 mL of PB (pH 6.0). Then, 50 μg of the anti-*Salmonella* pAbs and 200 μg of the catalases were successively added, followed by rotating at room temperature for 1 h. Then, 150 μL of EDC (1 mg·mL^{-1}) was prepared and immediately added into the mixture. After incubation for 30 min, the mixture was blocked with 1 mL of 2% (m/v) BSA for 1 h. Finally, the mixture was centrifuged at 7000 rpm for 10 min, re-suspended in 1 mL of PBS (pH 7.4, containing 1% BSA) and stored at 4 °C for further use.

Preparation of the mAb modified magnetic nanoparticles (MNPs)

The anti-*Salmonella* monoclonal antibodies were first modified with biotin using the biotin labeling kit (Elabscience, China, https://www.elabscience.com) according to the manufacturer's protocol. Then, 200 μg of the streptavidin modified MNPs were mixed with 40 μg of the biotinylated mAbs and incubated for 45 min at 15 rpm, followed by washing with PBST to remove the surplus antibodies. The immune MNPs were finally suspended in 500 μL of PBS (pH 7.4, containing 1% BSA), and stored at 4 °C for further use.

Separation and detection of the target bacteria

First, 50 μL of the immune MNPs was incubated with 500 μL of *Salmonella* at different concentrations (10^2–10^6 CFU·mL^{-1}) for 45 min at 15 rpm to form the MNP-*Salmonella* complexes. Then, the mixtures were magnetic separated for 2 min to remove the background and washed with 500 μL of PBST for further avoid non-specific binding. After the MNP-*Salmonella* complexes were re-suspended with 460 μL of PBS, 40 μL of the pAb-PS-catalase complexes were added and incubated for 1 h at 15 rpm to form the MNP-*Salmonella*-PS-catalase complexes. The complexes were then magnetically separated for 2 min and washed with 500 μL of PBST for four times to remove the unbound PSs. After the complexes were re-suspended with 40 μL of PBS, 20 μL of them were pipetted into the sample chamber of the microfluidic immunosensor, and detected by this immunosensor.

Results and discussions

Simulation and experiment of the micromixer in the microfluidic chip

The mixing efficiency of the micromixer has great impact on the detection time and sensitivity of this immunosensor. It was evaluated using the finite element analysis (FEA) software COMSOL (5.3a, Burlington, MA, USA) and shown in

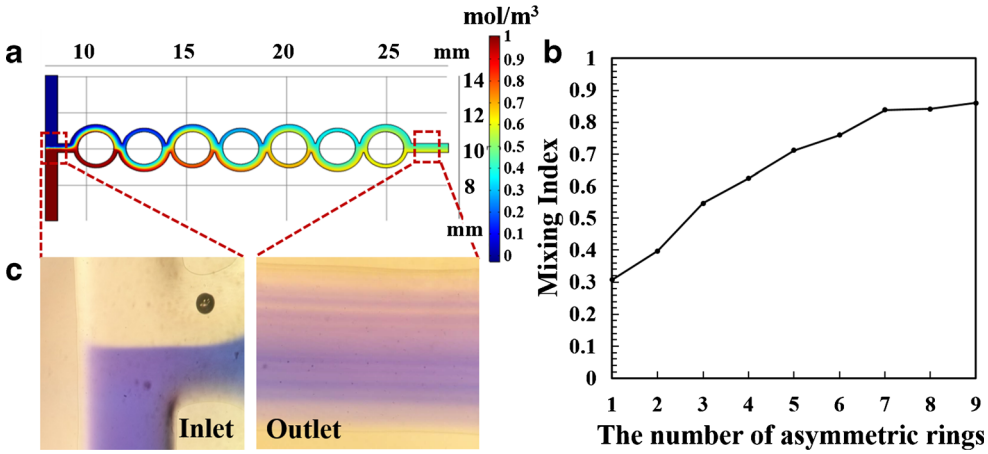

Fig. 2 **a** The numerical simulation results of the micromixer; **b** The mixing efficiency for different numbers of asymmetric rings; **c** The experimental results of the micromixer

Fig. 2a. To evaluate the degree of mixing in the micromixer, the simulated mixing efficiency (M_s) at the cross section of the mixing channel is defined as follows [26]:

$$M_s = 1 - \frac{\sqrt{\frac{1}{n}\sum_{i=1}^{n}(c_i - c_m)^2}}{c_m} \quad (1)$$

where, c_i is the concentration of the point *i*, c_m is the average concentration of all the points, and n is the total number of the points at the cross section. As shown in Fig. 2b, the mixing efficiency of this micromixer is able to reach about 85% when two fluids flow through seven asymmetric rings at the flow rate of 0.05 mL·min^{-1}, and does not increase obviously when more asymmetric rings are applied.

To compare the actual mixing effect of this developed micromixer with the simulation results, the blue dye solution and the PBS were injected with same flow rate (0.05 mL·min^{-1}) through the micromixer by syringe pump (Pump 11 Elite, Holliston, MA, USA, www.harvardbioscience.com.cn). The photos of the mixing at the inlet and outlet (shown in Fig. 2c) were taken by the microscope (Ti-E, Nikon, Tokyo, Japan, www.microscope.healthcare.nikon.com) with a CCD. The mixing performance of the micromixer is quantified by calculating the variance of the mixture concentration in a cross section of the mixing channel perpendicular to the flow direction and can be expressed as follows:

$$\sigma = \sqrt{\frac{1}{N-1}\sum_{i=1}^{N}\left(X_i - \overline{X}_i\right)^2} \quad (2)$$

$$M_e = 1 - \sqrt{\frac{\sigma^2}{\sigma_{max}^2}} \quad (3)$$

where, σ represents standard deviation, X_i represents the normalized color intensity of point i, $\overline{X}_i$ is the average color intensity and σ_{max} is the maximum standard deviation at the inlet. The experimental results were obtained using the image processing software (Image J) and show that this micromixer has a mixing efficiency of ~70% for two fluids. The numerical and experimental results indicate that the MNP-*Salmonella*-PS-catalase complexes and the pre-filled hydrogen peroxide can be well mixed by the modified passive micromixer to ensure the efficient enzymatic catalysis of hydrogen peroxide into oxygen.

Optimization of the distance indication

This microfluidic immunosensor was based on the visible indication of the travel distance of the red dye resulting from the catalyzed oxygen. Several factors have impact on the sensitivity of this immunosensor, including the amount of the catalase and pAbs modified PSs, the size of the distance indication channel, the reaction temperature and time. At first, three indication channels with different sizes of 600 × 300 μm (width × height), 300 × 150 μm and 150 × 75 μm were fabricated to detect the target bacteria at the same concentration of 1.0 × 10^6 CFU·mL^{-1}. As shown in Fig. 3a, the channel with the size of 300 × 150 μm had the longest travel distance (~ 150 mm) of the red dye in 5 min. In contrast, the channel with the size of 600 × 300 μm showed the shortest travel distance (~21 mm) due to the biggest cross-section size and the same volume of the catalyzed oxygen. However, an interesting phenomenon was observed that the channel with the size of 150 × 75 μm had a shorter distance than the one with 300 × 150 μm. This was due to the clogging of the channel with 150 × 75 μm (as shown in Fig. 3b) and a higher pressure was required to push the red dye. Thus, the optimal cross-section size of the indication channel was selected as 300 × 150 μm in this study.

Besides, the amount of the catalase and pAbs modified PSs was optimized using the optimal distance indicator with the channel of 300 × 150 μm. Different amounts of the PSs

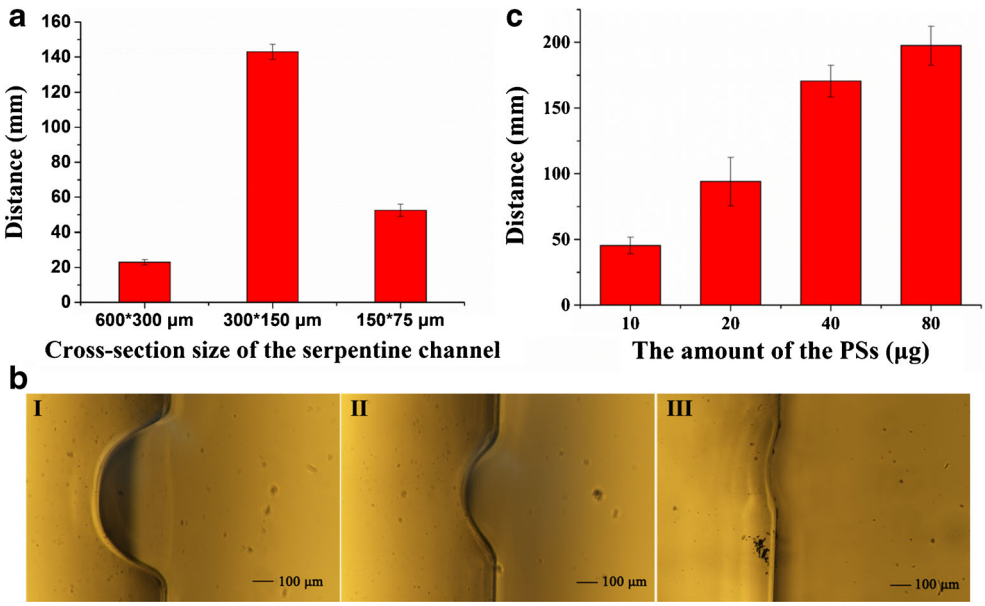

Fig. 3 **a** Optimization of the channel of the distance indicator; **b** Cross-sectional images of three serpentine channels with different dimensions (I, 600 × 300 μm; II, 300 × 150 μm; III, 150 × 75 μm); **c** Optimization of the amount of the PSs

ranging from 10 μg to 80 μg were used to detect the target bacteria at the same concentration of 1.0×10^6 CFU·mL^{-1} in 5 min. As shown in Fig. 3c, the travel distance increases dramatically from 45.5 mm for 10 μg of the PSs to 163.0 mm for 40 μg of the PSs, and does not increase very obviously, when more amount of the PSs were used. This indicates that 40 μg of the PSs are sufficient for conjugating with the MNP-*Salmonella* complexes. 10 μg of the PSs are too less for the catalases on these complexes to obtain sufficient O_2 and result in much less pressure to push the red dye to move. Thus, the optimal amount of 40 μg for the PSs was used in this study.

The pressure change in the chip was also very important in this method. The pressure change with different reaction temperatures and time was observed using 40 μg of catalase modified PSs and 0.5 M H_2O_2. As shown in Fig. S2, when the pressure in the chip was directly read out using the pressure meter, it is found that the increasing speed of the pressure in the chip becomes slower after 5 min. Thus, the optimal reaction time of 5 min was used in this study. The pressure in the chip were also measured at different temperatures. It is observed that the pressure change is only slightly more at 37 °C than at room temperature (25 °C) and much more than at other temperatures. Thus, the optimal reaction temperature was selected at room temperature in this study.

Detection of *S.* Typhimurium in pure cultures and chicken samples

To evaluate this microfluidic immunosensor for rapid detection of foodborne bacteria, three parallel tests on *S.* Typhimurium at different concentrations of 1.2×10^2 to 1.2×10^6 CFU·mL^{-1} in the pure cultures were conducted under the optimal conditions. The results are shown in Fig. 4a, and it is obviously seen that the higher concentration of the target bacteria has the longer travel distance. As shown in Fig. 4b, a good linear relationship between the travel distance (***D***) of the red dye and the concentration (***C***) of the bacteria from 1.2×10^2 to 1.2×10^5 CFU·mL^{-1} in the pure cultures was obtained and expressed as $\boldsymbol{D} = 19.601 * \lg(\boldsymbol{C}) + 26.817$ (R^2 = 0.992). Five negative samples were also tested as control to determine the lower detection limit of this immunosensor. Based on three times of signal to noise ratio, the detection limit was calculated as 1.5×10^2 CFU·mL^{-1}. Transmission electron microscope (TEM) imaging was performed to confirm the successful forming of the MNP-*Salmonella*-PS-catalase complexes (see Fig. 4c). As shown in Table 1, this immunosensor is more convenient and easier to detect *Salmonella* visually than most of recently reported methods.

To evaluate the applicability of this immunosensor for the detection of *S.* Typhimurium in real samples, *S.* Typhimurium at different concentrations of 1.2×10^2 to 1.2×10^6 CFU·mL^{-1} were prepared and added into the *Salmonella*-free chicken samples according to the protocol in Section 2.4, and three parallel tests on the spiked chicken samples were carried out using this immunosensor. As shown in Table 2, the recoveries for *S.* Typhimurium with the concentrations of 1.2×10^2 CFU·mL^{-1}, 1.2×10^3 CFU·mL^{-1}, 1.2×10^4 CFU·mL^{-1}, 1.2×10^5 CFU·mL^{-1} and 1.2×10^6 CFU·mL^{-1} are 114.6%, 99.9%, 98.0%, 101.5% and 106.4%, respectively. The mean recovery is 103.9%, indicating the feasibility of this immunosensor for the detection of *S.* Typhimurium in chicken samples. The signals of the spiked chicken samples were generally stronger than the pure culture due to the nonspecific

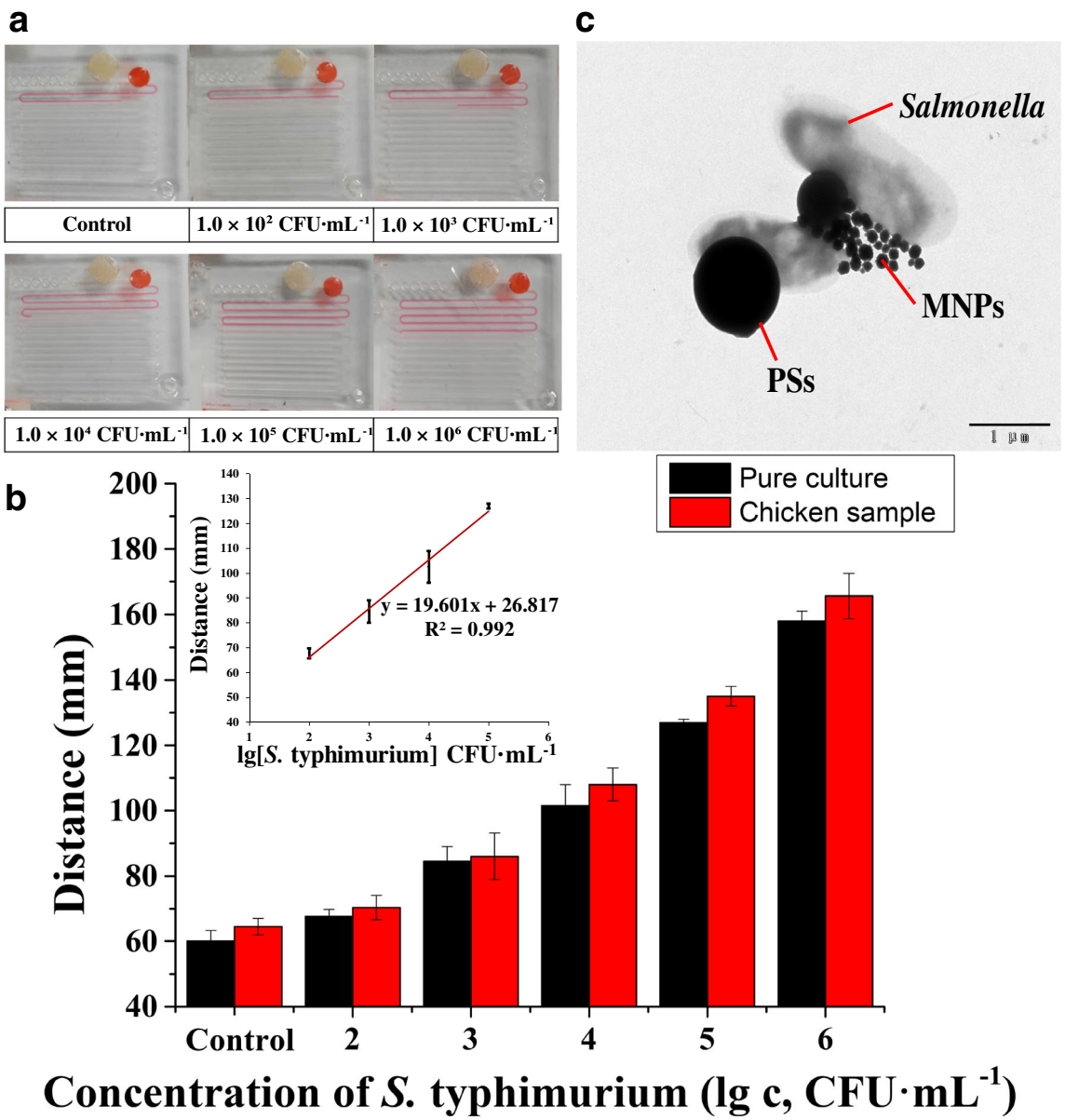

Fig. 4 **a** Travel distance of the red dye for *Salmonella* at different concentrations in pure cultures; **b** Detection of different concentrations of *Salmonella* in pure cultures and chicken samples. Inset shows the linear relationship between the travel distance of the red dye and log of concentrations of *S.* typhimurium in pure cultures; **c** TEM image of the MNP-*Salmonella*-PS-catalase complexes

Table 1 Comparison of this method to the reported methods for detection of *Salmonella*

Analytical method	Target	Linear range ($CFU \cdot mL^{-1}$)	Detection limit ($CFU \cdot mL^{-1}$)	Reference
Electrochemical	*Salmonella* typhimurium	10^3–10^7	500	[27]
Fluorescence	*Salmonella* enteritidis	10^2–10^5	300	[28]
SPR	*Salmonella*	10^2–10^7	60	[29]
Fluorescence	*Salmonella* aureus	10^2–10^5	100	[30]
Magnetic	*Salmonella enterica*	10^4–10^8	100	[31]
Lateral flow immunoassay	*Salmonella*	10^4–10^9	10,000	[32]
Visual	*Salmonella* typhimurium	10^2–10^6	150	This work

Table 2 The recovery of *S.* Typhimurium at the concentrations of 1.2×10^2–1.2×10^6 CFU·mL^{-1}

S. Typhimurium concentration (CFU·mL^{-1})	Travel distance for the chicken samples (mm)	Travel distance for the pure cultures (mm)	Recovery	CV
1.2×10^2	70	68	114.6%	3.87%
1.2×10^3	86	84	99.2%	8.27%
1.2×10^4	108	102	98.0%	4.72%
1.2×10^5	135	127	101.5%	2.22%
1.2×10^6	166	158	106.4%	4.13%

adsorption of the impurities in the chicken samples such as proteins and fats.

Specificity of the assay

The specificity of this immunosensor mainly depended on the anti-*Salmonella* monoclonal and polyclonal antibodies. Thus, three parallel tests on negative controls (PBS), *S.* Typhimurium, *S.* derby, *S.* enteritidis, *E. coli* O157: H7 and *Listeria monocytogenes* at the same concentration of 10^6 CFU·mL^{-1} were conducted to evaluate the specificity of the immunosensor. As shown in Fig. 5, the travel distance for non-target bacteria is almost the same with that for the negative controls. The travel distance of *S.* Typhimurium (~ 160 mm) is obviously longer than others, indicating that this immunosensor has a good specificity.

Conclusions

A microfluidic immunosensor combining with immunomagnetic separation, enzymatic catalysis and distance indication for rapid and sensitive detection of *S.* Typhimurium was successfully developed. The pressure increase caused by the catalytic dissociation of H_2O_2 by catalase on the bacteria pushed the pre-filled red dye to travel along the channel and its travel distance was visually observed to determine the bacterial concentration. This immunosensor showed a great performance in the detection of *S.* Typhimurium with good sensitivity and specificity. However, the incubation and magnetic separation steps were still performed outside the chip and required additional equipment, which will be further studied for in-field applications. The merits of this immunosensor, such as simple operation, easy readout and low cost, demonstrated that it has great potential to realize rapid and cost-effective detection of pathogens.

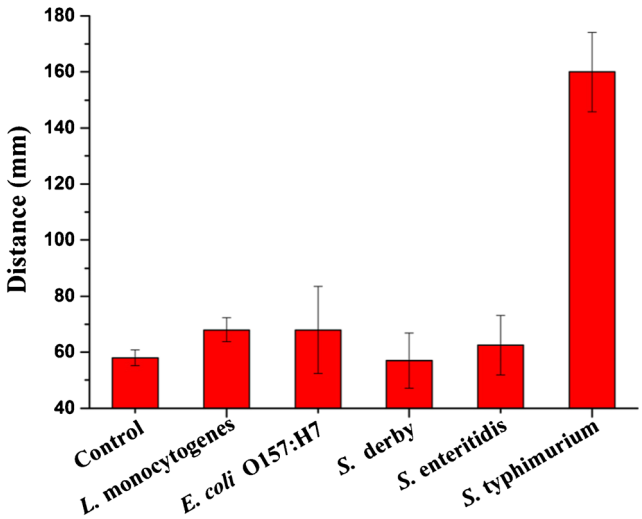

Fig. 5 The specificity of the microfluidic immunosensor

Acknowledgments This study was supported in part National Natural Science Foundation of China (31802219) and Walmart Foundation (SA17031161). The authors would like to thank Walmart Food Safety Collaboration Center for its great support.

Compliance with ethical standards

Conflict of interest The authors declare that they have no conflict of interest.

References

1. Rubab M, Shahbaz HM, Olaimat AN, Oh D-H (2018) Biosensors for rapid and sensitive detection of Staphylococcus aureus in food. Biosens Bioelectron 105:49–57
2. WHO, Food safety, http://www.who.int/en/news-room/fact-sheets/detail/food-safety, 2017
3. Zhao X, Lin CW, Wang J, Oh DH (2014) Advances in rapid detection methods for foodborne pathogens. J Microbiol Biotechnol 24(3):297–312
4. Mandal PK, Biswas AK, Choi K, Pal UK (2011) Methods for rapid detection of foodborne pathogens: an overview. Am J Food Technol 6(2):87–102
5. Wang M, Yang J, Gai Z, Huo S, Zhu J, Li J, Wang R, Xing S, Shi G, Shi F, Zhang L (2017) Comparison between digital PCR and real-time PCR in detection of Salmonella typhimurium in milk. Int J Food Microbiol 266:251–256
6. Mao Y, Huang X, Xiong S, Xu H, Aguilar ZP, Xiong Y (2016) Large-volume immunomagnetic separation combined with multiplex PCR assay for simultaneous detection of Listeria monocytogenes and Listeria ivanovii in lettuce. Food Control 59:601–608
7. Kim J, Kim H, Park JH, Jon S (2017) Gold Nanorod-based photo-PCR system for one-step, rapid detection of Bacteria. Nanotheranostics 1(2):178–185
8. Bennett RW (2005) Staphylococcal enterotoxin and its rapid identification in foods by enzyme-linked immunosorbent assay-based methodology. J Food Prot 68(6):1264
9. Tu Z, Chen Q, Li Y, Xiong Y, Xu Y, Hu N, Tao Y (2016) Identification and characterization of species-specific nanobodies for the detection of Listeria monocytogenes in milk. Anal Biochem 493:1–7
10. Ahmed A, Rushworth JV, Hirst NA, Millner PA (2014) Biosensors for whole-cell bacterial detection. Clin Microbiol Rev 27(3):631–646

11. Magiati M, Sevastou A, Kalogianni DPJMA (2018) A fluorometric lateral flow assay for visual detection of nucleic acids using a digital camera readout. Microchim Acta 185(6):314
12. Yoo SM, Lee SY (2016) Optical biosensors for the detection of pathogenic microorganisms. Trends Biotechnol 34(1):7–25
13. Ramon-Marquez T, Medina-Castillo AL, Fernandez-Gutierrez A, Fernandez-Sanchez JF (2016) A novel optical biosensor for direct and selective determination of serotonin in serum by solid surface-room temperature phosphorescence. Biosens Bioelectron 82:217–223
14. Pastucha M, Farka Z, Lacina K, Mikusova Z, Skladal P (2019) Magnetic nanoparticles for smart electrochemical immunoassays: a review on recent developments. Mikrochim Acta 186(5):312
15. Nabaei V, Chandrawati R, Heidari H (2018) Magnetic biosensors: Modelling and simulation. Biosens Bioelectron 103:69–86
16. Rong Z, Wang C, Wang J, Wang D, Xiao R, Wang S (2016) Magnetic immunoassay for cancer biomarker detection based on surface-enhanced resonance Raman scattering from coupled plasmonic nanostructures. Biosens Bioelectron 84:15
17. Yuan M, Zhang Q, Song Z, Ye T, Yu J, Cao H, Xu F (2019) Piezoelectric arsenite aptasensor based on the use of a self-assembled mercaptoethylamine monolayer and gold nanoparticles. Microchim Acta 186(5):268
18. Pohanka M (2018) Piezoelectric biosensor for the determination of tumor necrosis factor alpha. Talanta 178:970–973
19. Chen Y, Chu W, Liu W, Guo X (2018) Distance-based carcinoembryonic antigen assay on microfluidic paper immunodevice. Sensors Actuators B Chem 260:452–459
20. Tian T, Li J, Song Y, Zhou L, Zhu Z, Yang CJ (2016) Distance-based microfluidic quantitative detection methods for point-of-care testing. Lab Chip 16(7):1139–1151
21. Wang Y, Zhu G, Qi W, Li Y, Song Y (2016) A versatile quantitation platform based on platinum nanoparticles incorporated volumetric bar-chart chip for highly sensitive assays. Biosens Bioelectron 85: 777–784
22. Xie Y, Wei X, Yang Q, Guan Z, Liu D, Liu X, Zhou L, Zhu Z, Lin Z, Yang C (2016) A Shake&Read distance-based microfluidic chip as a portable quantitative readout device for highly sensitive point-of-care testing. Chem Commun 52(91):13377–13380
23. Liu D, Li X, Zhou J, Liu S, Tian T, Song Y, Zhu Z, Zhou L, Ji T, Yang C (2017) A fully integrated distance readout ELISA-Chip for point-of-care testing with sample-in-answer-out capability. Biosens Bioelectron 96:332–338
24. Ansari MA, Kim K-Y, Anwar K, Kim SM (2010) A novel passive micromixer based on unbalanced splits and collisions of fluid streams. J Micromech Microeng 20(5):055007
25. Chen Y, Xianyu Y, Wu J, Dong M, Zheng W, Sun J, Jiang X (2017) Double-enzymes-mediated bioluminescent sensor for quantitative and ultrasensitive point-of-care testing. Anal Chem 89(10):5422–5427
26. Li J, Xia G, Li Y (2013) Numerical and experimental analyses of planar asymmetric split-and-recombine micromixer with dislocation sub-channels. J Chem Technol Biotechnol 88(9):1757–1765
27. Dong J, Zhao H, Xu M, Ma Q, Ai S (2013) A label-free electrochemical impedance immunosensor based on AuNPs/PAMAM-MWCNT-chi nanocomposite modified glassy carbon electrode for detection of Salmonella typhimurium in milk. Food Chem 141(3): 1980–1986
28. Liu K, Yan X, Mao B, Wang S, Deng L (2015) Aptamer-based detection of Salmonella enteritidis using double signal amplification by Klenow fragment and dual fluorescence. Microchim Acta 183(2):643–649
29. Lei P, Tang H, Ding S, Ding X, Zhu D, Shen B, Cheng Q, Yan Y (2014) Determination of the invA gene of Salmonella using surface plasmon resonance along with streptavidin aptamer amplification. Microchim Acta 182(1–2):289–296
30. Juronen D, Kuusk A, Kivirand K, Rinken A, Rinken T (2018) Immunosensing system for rapid multiplex detection of mastitis-causing pathogens in milk. Talanta 178:949–954
31. Cheng Y, Xianyu Y, Wang Y, Zhang X, Cha R, Sun J, Jiang X (2015) One-step detection of pathogens and viruses: combining magnetic relaxation switching and magnetic separation. ACS Nano 9(3):3184–3191
32. Liu CC, Yeung CY, Chen PH, Yeh MK, Hou SY (2013) Salmonella detection using 16S ribosomal DNA/RNA probe-gold nanoparticles and lateral flow immunoassay. Food Chem 141(3):2526–2532